Design, Optimization, and Fabrication of Side-Illuminated p-i-n Photodetectors With High Responsivity and High Alignment Tolerance for 1.3- and 1.55-μm Wavelength Use

Vincent Magnin, Louis Giraudet, Joseph Harari, J. Decobert, P. Pagnot, E. Boucherez, and Didier Decoster

***Abstract*—In this paper, we describe the design, optimization and fabrication of side-illuminated p-i-n photodetectors, grown on InP substrate, suitable for surface hybrid integration in low-cost modules. The targeted functionalities of these photodetectors were a very high responsivity at 1.3- and 1.55-μm wavelengths and quasi-independent on the optical polarization, and had a high alignment tolerance. Moreover, in order to avoid any reliability problem, the principle of evanescent coupling was adopted. Two photodetectors were optimized, fabricated, and tested; the first was for classical cleaved fiber, and the second was for lensed fiber. Because the considered epitaxial structures were complicated to optimize, the method of the genetic algorithm was used, associated with a beam propagation method (BPM). The photodetectors are based on multimode diluted waveguides, which are promising structures in the field of optoelectronics and integrated optics. Starting from the presented comparisons between experimental and theoretical results, the interest of the design method is discussed and the complete performances of newly fabricated devices are presented. The aspect of the cutoff frequency is also considered.**

***Index Terms*—Beam propagation method (BPM), diluted waveguide, evanescent coupling photodiode, genetic algorithm, multimode waveguide, optimization, reliability, waveguide photodiode.**

I. Introduction

FOR several years, the long wavelength p-i-n photodetectors have been object of attention because they are a key element in the future photonic circuits used for optical transmissions and measurement systems [1], [2]. Until now, the main functionalities of the device have been improved. The side-illuminated structures have demonstrated their interest; they allow for overcoming the well-known compromise between responsivity and cutoff frequency [1], [3]. High-frequency p-i-n photodetectors have then been fabricated [4]–[7]. In this case, for long wavelength use, the device core thickness is small, which makes it necessary to use a lensed fiber to get a high fiber-photodetector coupling efficiency, even when an optical multimode structure is used [3], [8]. On the other hand, the fiber–chip coupling has become a center of interest [9]–[18] and the side-illuminated structure allows us to use the same integration concept for the photodiode and the laser diode on a planar board. Under these conditions, the coupling efficiency between the photodiode and the fiber is of prime importance [19]–[23] and, as a consequence, so is the alignment tolerance when considering low-cost integration with flip-chip hybrid report. This is why we present, in this paper, the design, optimization, and fabrication of a new side-illuminated p-i-n photodiode grown on InP substrate whose properties are

1) a very high quantum efficiency (>0.9) at 1.3- and 1.55-μm wavelength;
2) a low sensitivity to vertical (and horizontal) misalignment;
3) a low sensitivity to optical polarization [transverse electric (TE) or transverse magnetic (TM)].

Moreover, because this photodiode has been designed to avoid the reliability problems involved in the passivation of the illuminated active facet [2], we adopted the principle of evanescent coupling, which demonstrated interesting performances [24]–[27]. Our first objective was not to obtain a very high frequency device, the expected cutoff frequency of this photodiode being around 3 GHz (for 2.5-Gb/s applications). This aspect will be discussed at the end of this paper. Because the epitaxial structure is complicated, such a photodetector is impossible to design easily step by step, and the design and optimization were performed using both the beam propagation method (BPM) and a genetic algorithm, a multiparameter optimization method being requisite to handle the numerous optimization parameters [28]. Under these conditions, the photodetector epitaxial structure can be precisely adapted to the illuminating fiber and to the targeted functionalities. First, we considered a photodetector suitable for classical cleaved fiber. The main objective was to get very high quantum efficiency and alignment tolerance. After this step, we attempted to reduce the photodiodes active region area in order to increase the cutoff frequency. This led us to design another structure suitable for a lensed fiber whose mode width is near 5 μm at 1.3-μm wavelength.

The first part of this paper presents the typical new epitaxial structure of the photodetector and the optimization method. It finally gives the optimum photodiode characteristics and the associated structure, which has been grown on InP substrate. The second part describes the device fabrication and characterization, with the comparison between experimental results and

Manuscript received February 15, 2001; revised November 21, 2001.

V. Magnin, J. Harari, and D. Decoster are with the Institut d'Electronique et de Microélectronique (IEMN), Villeneuve d'Ascq 59652, France.

L. Giraudet, J. Decobert, P. Pagnot, and E. Boucherez are with the OPTO+ Route de Nozay, Marcoussis 91460, France.

Publisher Item Identifier S 0733-8724(02)01011-3.

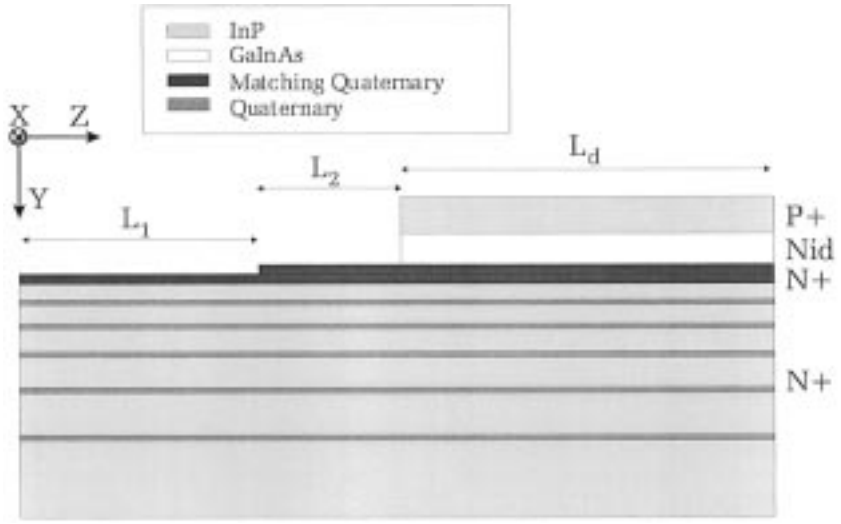

Fig. 1. Typical structure of the optically matched photodetector.

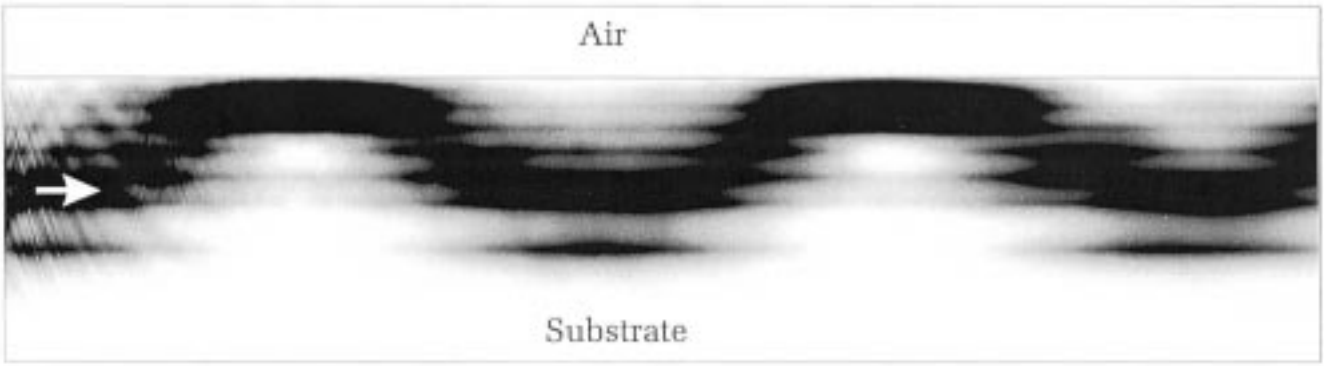

Fig. 2. Example of propagation of an optical beam in our type of waveguide. The total propagation length is 300 μm. The mode width is 5.1 μm at 1.3-μm wavelength in TE mode and the optical beam is injected 3 μm under the waveguide surface.

theoretical predictions. Finally, we conclude on the possible increase of the cutoff frequency of such a device.

II. Photodiode Epitaxial Structure and Optimization Method

A. Epitaxial Structure

The epitaxial structure is based on the classical superstructure of evanescent coupling photodiodes, that is a low-doped GaInAs epilayer inserted between a P^+ InP epilayer and a N^+ quaternary (GaInAsP) matching layer. However, here, the waveguide used to carry the light from the injection facet to the absorbing structure is made with a multimode diluted waveguide [11], [12], as presented in Fig. 1. The waveguide is made from very thin quaternary epilayers introduced in InP. From the electrical point of view, all waveguide epilayers have a high donor (N^+) concentration. The number of quaternary layers has a great influence on the photodetector performances. Moreover, as shown in Fig. 1, the distance between the quaternary layers decreases between the substrate and the top of the optical waveguide. This design was implemented to obtain a specific optical behavior, which can be compared to a half lens whose center is on the top of the optical waveguide. The optical beam introduced in this structure is focused and guided toward the top of the waveguide (see an example of beam propagation in Fig. 2). Then, to obtain the photodiode, the upper-structure of the photodetector with the absorbing and matching layers has to be placed precisely at the distance where light reaches the waveguide surface. Such a structure is difficult to optimize. The different parameters to know are

1) the quaternary composition (refractive index) and epilayer thickness;
2) the number of quaternary epilayers;
3) the distance (thickness) between these epilayers;
4) the matching layer quaternary type and thickness;
5) the absorbing layer thickness;
6) the lengths (L_1 & L_2) of the different parts of the waveguide (Fig. 1).

To simplify the optimization and the epitaxy, the quaternary layer thickness was kept equal for all thin layers. In the frame of this work, we considered large photodiodes (50 μm), the device length (L_d) also being an important parameter. The number of parameters leads us to use the method of the genetic algorithm in order to get one of the best possible devices. Considering now the objective, the first optimizations were used to get a high responsivity and high vertical alignment tolerance at 1.55-μm wavelength (TE polarization); then, we considered TE and TM polarizations. Finally, we added the same objectives at 1.3-μm

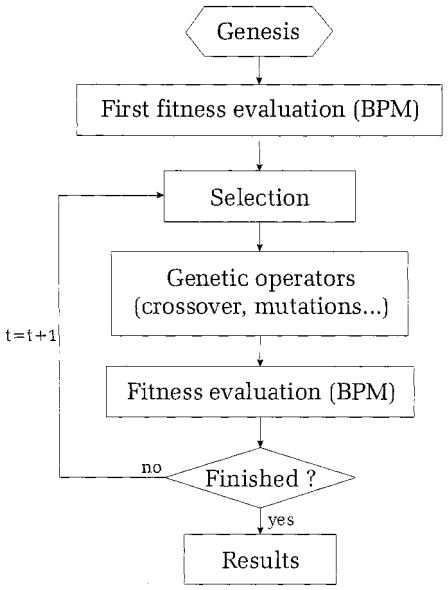

Fig. 3. Algorithm of the optimization method.

wavelength. At each step, by modifying the structure, we noticed that the photodiode performances were improved without reducing the performances obtained by previous optimizations. In other words, the best performances at 1.55 μm in TE polarization obtained with the first optimized structure are preserved in the last structure, which also has very good performances for TM polarization and at 1.3-μm wavelength. From a general point of view, a number of different types of waveguide structures were tested (with different quaternaries, or thick quaternary epilayers), the main goal being to fabricate a half lens. The structure that we present in this paper is the easier to fabricate by epitaxy. The total waveguide thickness is lower than 9 μm and, thus, can be fabricated easily because, for this type of structure, the epimaterial is mainly InP. Moreover, only two different quaternaries lattice matched to InP are needed.

The studied devices will be named according to their waveguide structures (epitaxial structure number and L_1 and L_2 parameters); for instance, structure 1-50-0 indicates a device with a number one epitaxial structure, $L_1 = 50\,\mu$m, and $L_2 = 0\,\mu$m.

B. Modeling Tool and Optimization Method

Genetic algorithms (GAs) are based on Charles Darwin's theory [29]–[32]. As natural selection achieved evolving complex organs and organisms amazingly well adapted to their environment, GAs can be used to evolve the numerous variables of a device until it offers the desired performances. They operate on a population of N devices, each being a potential solution to the problem. A device is represented by one or several binary strings, called chromosomes, coding for all variables of the problem. After the initialization of these variables during the genesis, the algorithm (see Fig. 3) consists mainly of a temporal loop, representing generations. Each device of the current generation is evaluated using a fitness function, which allows selecting the surviving part of the population. Couples of surviving mates are formed to generate offspring by a crossover operation on their chromosomes. Mutations also occur. As generations go on, the population fitness tends to ameliorate.

The physical model used to simulate the optical beam propagation in the photodetector is a classical two-dimensional (2-D) finite differences beam propagation method (BPM) with scalar and paraxial approximations [33], [34]. The two propagation equations that are solved for TE and TM modes are, respectively

$$\frac{\partial^2 E(x,z)}{\partial x^2} - 2i\beta \cdot \frac{\partial E(x,z)}{\partial z} + \left(k_0^2 \cdot n^2(x,z) - \beta^2\right) E(x,z) = 0 \quad (1)$$

$$\frac{\partial}{\partial x}\left(\frac{1}{n^2(x,y)}\frac{\partial}{\partial x}H(x,z)\right) - 2i\beta \cdot \frac{\partial H(x,z)}{\partial z} + \left(k_0^2 \cdot n^2(x,z) - \beta^2\right) H(x,z) = 0 \quad (2)$$

where E and H are, respectively, the electrical and magnetical fields of the optical wave, $n(x,z)$ is the refractive index at the position (x,z), β is the propagation constant, and k_0 is the wavenumber in a vacuum. In our approach, we designed the photodiode to be sufficiently wide to absorb the whole optical beam issued from the fiber and propagating in the waveguide. For this reason, the photodiode width has been experimentally set to 50 μm and the slab waveguide approximation is, therefore, valid. A horizontal taper can be designed but this was not our objective. In these conditions, the light propagation in the vertical plane was the most important aspect of the problem and we assumed the validity of a 2-D physical model. Moreover, the use of a GA supposes the capability to calculate more than 10 000 physical models and requires a fast BPM algorithm. This also explains the choice of a 2-D BPM instead of a three-dimensional (3-D) one. The fitness function used to evaluate each device at each generation step translates the user's desire into mathematical terms. In the case of multiobjective optimization [35], one simple solution is to consider q objective functions f_i and to combine them linearly in a unique fitness function using α_i weights

$$f = \sum_{i=1}^{q} \alpha_i \cdot f_i. \quad (3)$$

In our optimization, the four objective functions are the calculated photodetector quantum efficiencies at 1.3-μm and 1.55-μm wavelengths, in TE and TM modes

$$f = \frac{1}{4}\left(\eta_{1.3}^{\mathrm{TE}} + \eta_{1.3}^{\mathrm{TM}} + \eta_{1.55}^{\mathrm{TE}} + \eta_{1.55}^{\mathrm{TM}}\right). \quad (4)$$

During our work, we tested several fitness functions (products, summations of products, and geometrical average) by optimizing each time and comparing the properties of the best device after optimization. All of these functions give the same importance to each targeted property (a very high responsivity at 1.55 and 1.3 μm and for all optical polarizations). Among the different types of fitness functions, we observed that the linear combination allowed to get the best device. The algorithm begins with genesis (Fig. 3), which initializes the first generation. The optimization variables are chosen and the search space is defined. Each variable is limited to a finite range that is discretized. This allows the binary coding of

Fig. 4. Principle of crossover.

each variable as a 32-bit-long integer. The population size was fixed at 100 devices (we tested 50, 100, 200, and 300). This is sufficient to distribute the first population all over the search space. A larger population increases the calculation time without improving the optimization result. After selection, each couple generates two children devices by application of a crossover operator. Among the numerous existing techniques, we use a two-point-crossover operator [36]; the corresponding chromosomes of each mate are identically cut at two random positions and cross recombined to produce two new chromosomes (see Fig. 4). Resulting children are different from their parents but share some of their characteristics. Mutations also occur during reproduction. They consist of a random inversion of a bit of a chromosome. A mutation probability P_m per bit and per generation is defined and a self-adaptation technique is used [37]. Each device has its own mutation probabilities for each variable. They are coded in a second chromosome that is submitted to the same crossover and mutation operators as the main one. Consequently, mutation probabilities can adapt themselves to the problem and follow their own evolution. If a given mutation probability is too high, the risk of degrading the device will be important. If it is too low, the evolution of the corresponding gene is penalized. This technique allows the algorithm to adapt automatically the mutations during optimization [37].

The optimization can be stopped after 100–150 generations, in our case. Fig. 5 shows the evolution of the population fitness distribution during optimization. The mutation technique avoids too fast a homogenization of the population, and so allows the exploration of the entire search space as much as possible. A complete optimization needs 20 000–30 000 BPM runs (four BPM runs per device and per generation). This is realized in one or two days in Fortran language on an up-to-date personal computer.

C. Optimized Structures

The first optimized photodetector is aiming at cleaved fiber coupling. The optical characteristics of this fiber considered in the simulation are a 9.0-μm mode width (at $1/e$) at 1.3-μm wavelength and 10.5 μm at 1.55 μm. Some of the parameters have been fixed from the beginning due to the fact that the photodetector has to follow a scheme of hybrid surface integration. In particular, the vertical position of the fiber axis was fixed at 5 μm below the waveguide surface. The aspect of the frequency response was not considered provided that the photodetector is able at work up to 2.5 Gb/s. Consequently, the photodiode maximum length was fixed at 200 μm. Concerning the quaternary composition, several trials were made for all optimized structures, demonstrating that this parameter can be fixed at the beginning without degrading the final device properties. Taking into account epitaxial facilities, we chose the 1.05-μm wavelength quaternary (Q1.05) lattice matched to InP. After several optimization runs, the number of quaternary epilayers in the waveguide structure was fixed at eight, which leads to a good compromise between the total epitaxial thickness and the final performances. The length of the input waveguide was fixed at 50 μm. These parameters being defined, the search space of the first structure is given in Table I. Structure 1 has eight waveguide quaternary layers with the same thickness and eight waveguide InP layers with different thicknesses. A final important aspect concerning the evanescent coupling photodetector (that is, the photodetector with input waveguide) is the need for a small electron-hole pairs generation rate in the first micrometers of the photodiode, in order to avoid problems near the vertically etched photodetector mesa (passivation and low frequency cutoff due to low field effect). This aspect was taken into account when choosing the final optimized structure, which is presented in Table II; on the left is the top of the structure, and on the right is the substrate. We have successively put the photodiode, the matching layer, and the waveguide. All thicknesses are shown in micrometers.

Structure 2 was designed for a lensed fiber developed at OPTO+ (Marcoussis 91460, France), whose mode diameters are 5.1 and 5.5 μm, respectively, at 1.3 and 1.55 μm. The fiber axis position was fixed at 3 μm below the waveguide surface and there were eight thin quaternary epilayers. After several trials, the matching epilayers were made with the 1.18-μm wavelength quaternary lattice matched to InP. This structure is presented in Table III; on the left is the top of the structure, and on the right is the substrate. We have successively put the photodiode, the matching layers, and the waveguide. All thicknesses are shown in micrometers.

In structure 2, the two matching layers are thicker than in structure 1 and an InP thin epilayer is used as an etch stop. The search space was the same as in structure 1. The only difference is that matching layers can be thicker (up to 2 μm). A TE modal analysis in the vertical plane (Figs. 6 and 7) demonstrates that waveguide 1 has three modes, whereas the second one has only two modes. In each case, the first mode overlaps the second one at the center of the waveguide, where the fiber has to be set. The second mode (and third mode, if it exists) has a large extension toward substrate. This property is obviously related to the fact that the thin quaternary epilayers constitute a multiple diluted waveguide [11]. The beat effect between the first two modes explains the optical behavior of Fig. 2, as in multimode-interference (MMI) devices, for example. A comparison of Figs. 6 and 7 shows that if we consider the first two modes, the optimized waveguides have a similar modal distribution. The main difference is the mode extension. The particular structure of these multimode diluted waveguides (MDW) allows the enlargement of the width of each mode in order to get very high coupling efficiency with different input fibers while relaxing the alignment constraints. The material refractive indexes introduced in our work are from [38]–[42].

Let us consider now the influence of the waveguide characteristics for both structures. At the end of the optimization process, among the best structures we found, we chose those for

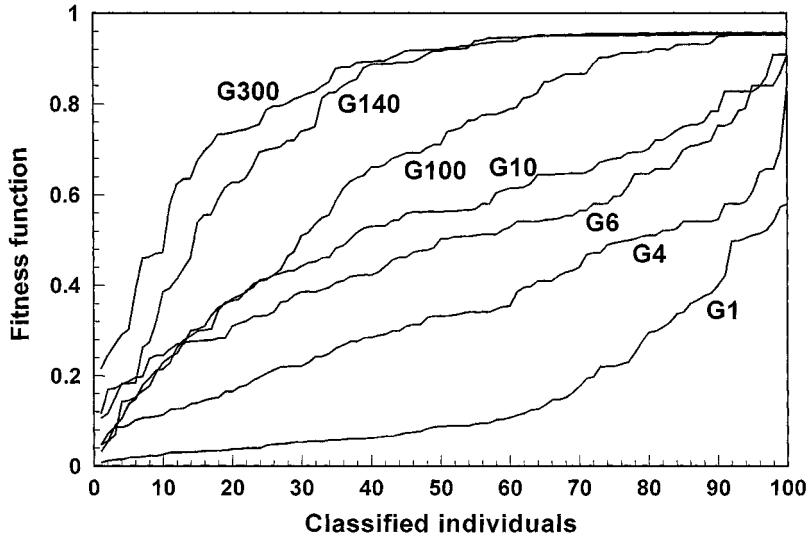

Fig. 5. Fitness distribution during evolution at different generations.

TABLE I
SEARCH SPACE FOR STRUCTURE 1

Layer	InP (top)	GaInAs	Matching Quat.	Waveg. Quat.	Waveg. InP
Search space	[0.5 μm , 2 μm]	[0.5 μm , 2 μm]	[0 μm , 1 μm]	[0.02 μm , 0.2 μm]	[0 μm , 2 μm]

TABLE II
EPITAXIAL STRUCTURE FOR CLEAVED FIBER

Photodiode			Waveguide																
InP	GaInAs	Q1.05	InP	Q1.05	InP	Q1.05	InP	Q1.05	InP	Q1.05	InP	Q1.05	InP	Q1.05	InP	Q1.05	InP	Q1.05	InP
0.92	2.0	0.48	0.42	0.10	0.38	0.10	0.54	0.10	0.70	0.10	0.84	0.10	0.84	0.10	1.02	0.10	1.68	0.10	sub

TABLE III
EPITAXIAL STRUCTURE FOR LENSED FIBER

Photodiode					Waveguide														
InP	GaInAs	Q1.18	InP	Q1.18	InP	Q1.05	InP	Q1.05	InP	Q1.05	InP	Q1.05	InP	Q1.05	InP	Q1.05	InP	Q1.05	InP
1	2.0	0.35	0.02	1.6	0.10	0.14	0.10	0.14	0.25	0.14	0.38	0.14	0.43	0.14	0.50	0.14	0.50	0.14	1	0.14	sub

which $L2 = 0$ in order to simplify the technology. Considering the waveguide length, the typical optical behavior presented in Fig. 2 allows an understanding that the photodetector responsivity is maximized for a certain waveguide length value giving a good optical beam confinement toward the absorbing layer. In fact, the optical beam propagates in the vicinity of the waveguide top over a certain distance (Fig. 2). This explains that, for waveguide lengths between 30 and 100 μm, the photodetector quantum efficiency for both wavelengths varies by only a few percent. The maximum is near 50 μm.

III. PHOTODETECTOR PERFORMANCES

A. Fabrication and Characterization Method

The epitaxial structures were grown by low-pressure metal organic vapor phase epitaxy (MOVPE). Special care was taken to control the different layer thicknesses, and several tools were used to measure the actual layer thicknesses. In particular, calibration of GaInAsP–InP growth rates (with GaInAsP 1.05-μm wavelength) was performed using super-lattices and X-ray rocking curve analysis. This allows precise control of the diluted input waveguide thickness. For the top GaInAs absorption layer and the upper GaInAsP matching layer, the thickness was measured after device mesa formation using a conventional surface profiler. In the case of structure 2, an etch stop was inserted between the lower and upper GaInAsP waveguide layers in order to control both thicknesses during device fabrication. The different thicknesses were also measured on cleaved samples using an e-beam microscope.

The fabrication sequence is simple. After top p-contact deposition and annealing, the metal is used as a mask for wet chemical etching of the top InP and GaInAs layers. Then, a second lithography step is performed, followed by another wet chemical etching of the matching GaInAsP layer, down to the

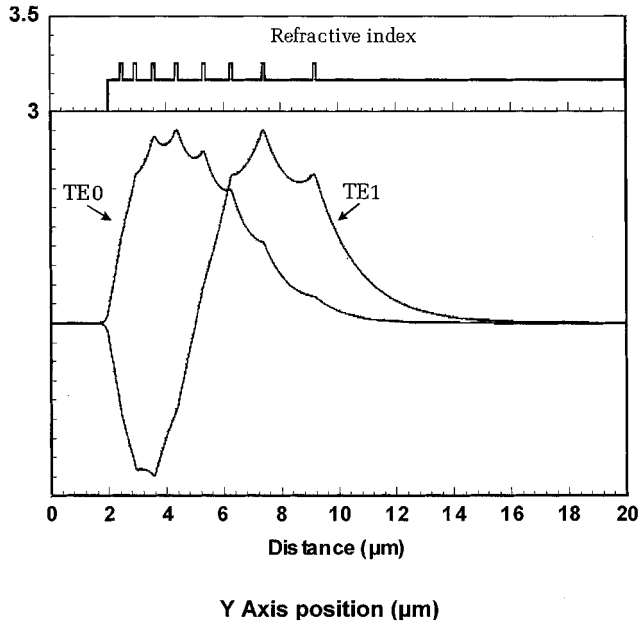

Fig. 6. Modal analysis of structure 1 (TE modes) at 1.55-μm wavelength. The third mode is not shown.

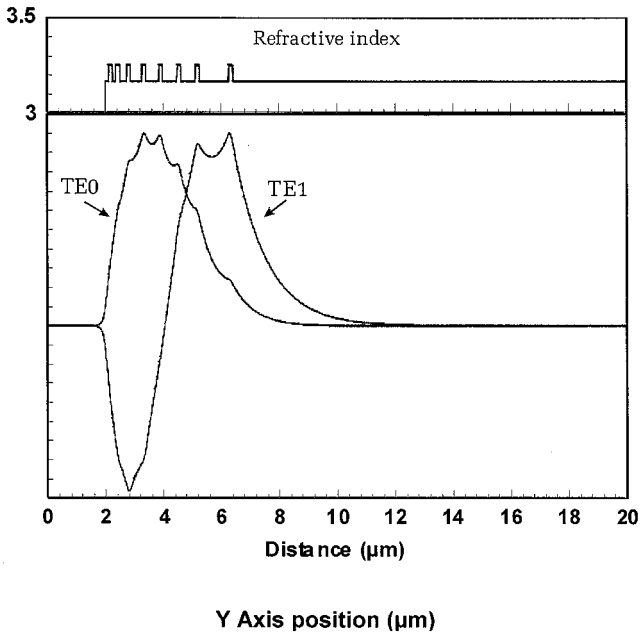

Fig. 7. Modal analysis of structure 2 (TE modes) at 1.55-μm wavelength.

InP layer. Finally, the substrate is thinned and the devices are cleaved using alignment marks to allow a waveguide length precision of about ± 5 μm that can be checked after the operation.

By appropriately shifting the waveguide mesa and the photodiode mesa from one device to another, all of the waveguide lengths studied here are realized in a single cut (as shown later in Fig. 11). The photodiode mesa is 50-μm-wide for all devices, and the diode lengths vary from 50 to 200 μm. No lateral confinement of the light is performed (planar waveguide). The low lateral divergence of the light in the semiconductor allows all the light to be absorbed by the 50-μm-wide diodes, even in the longest devices.

The measurement setup consists of an XYZ piezoelectric positioner with automatic fiber alignment capability in order to precisely align the fiber in front of the detector and to measure the fiber position tolerances. It is worth noticing the absence of absolute control of the fiber position in front of the epitaxial structure (optical fiber axis position with respect to epilayer). The state of polarization is changed by using a simple Lefevre setup. For this reason, we do not know the polarization of the input optical signal but we can measure the effects of the polarization change. The optical power is measured at the fiber output (cleaved or lensed) using the large surface detector of a calibrated optical power meter. The precision is estimated to be about 10%, mostly due to the calibration uncertainty. After the photocurrent is measured, the responsivity can be easily deduced. The same sequence is applied at 1.32 and 1.56 μm. All experiment–theory comparisons in this paper have been obtained following the same method. The experimental results are directly reported in the graph containing theoretical curves with only the two following corrections (Figs. 12, 16, 17). First, the experimental responsivity is divided by the classical factor 0.71 to compensate the reflection at the air–device interface. Second, because of lack of control of the absolute fiber position in the experimental setup, the experimental X axis reference ($X = 0$ μm) is adjusted to match with the theoretical results.

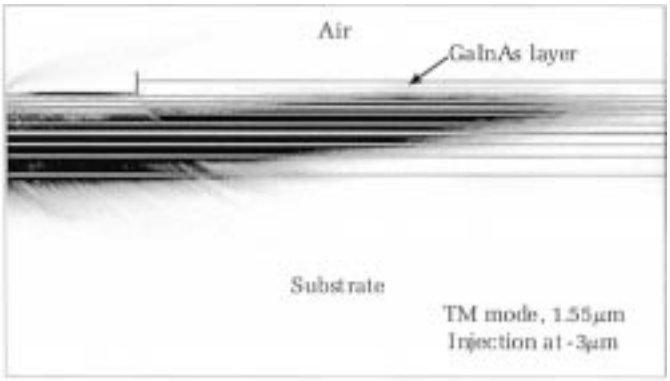

(a)

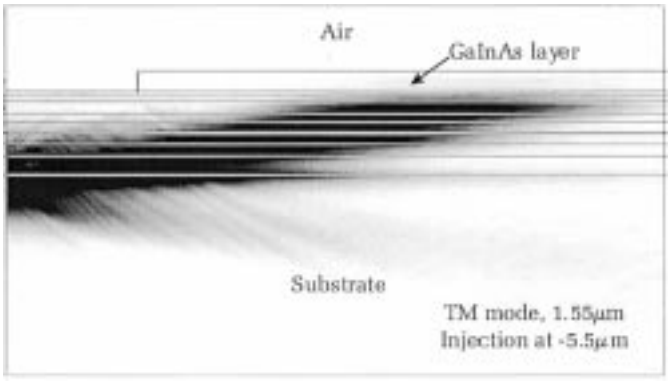

(b)

Fig. 8. Propagation of the light beam in structure 1 in (a) a cleaved fiber aligned on the waveguide axis (-5 μm from waveguide surface) and (b) a fiber with 2.5 μm misalignment toward substrate. The window is 250-μm long and 35-μm high.

B. Structure 1 for Cleaved Fiber

The simulated optical behavior of structure 1 is showed in Fig. 8 for the two cases of a fiber positioned 5 μm below the surface, and a fiber with a 2.5-μm vertical misalignment toward

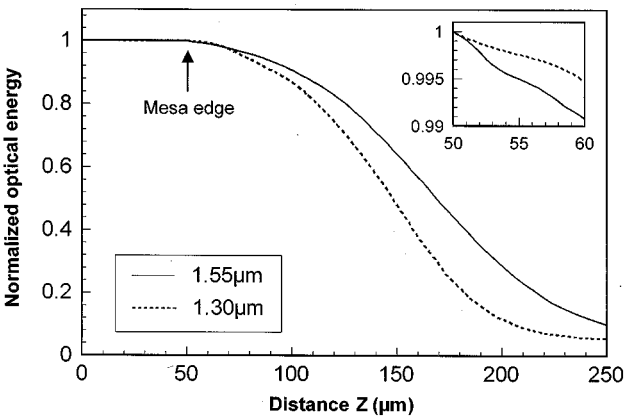

Fig. 9. Absorption process in the structure 1-50-0 at 1.55- and 1.3-μm wavelength (TE mode). Insert: t absorption process in the first micrometers of the photodiode.

the substrate (7.5 μm below the surface). This allows an appreciation of the capability of this waveguide structure to deal with misalignments. Indeed, in the second case, only a small part of the input optical beam is lost in the substrate. The absorption process of this photodetector is presented in Fig. 9, with an insert showing the small optical energy absorbed in the first micrometers of the photodiode. These results can be compared to the well known behavior of the classical waveguide p-i-n photodetector [8], where most of the input optical beam is absorbed within the first five micrometers. On the contrary, the structure presented here has a very small carrier generation rate near the photodiode mesa edge. This is possible thanks to the evanescent coupling, which smoothes the absorption process along the whole photodiode length. This particular aspect is promising concerning power behavior but it will be problematic when attempting to get a high-frequency photodetector (more than 20 GHz) based on the epitaxial structure 1.

To describe more precisely the behavior of this structure, we have calculated its average quantum efficiency versus fiber vertical position for three fiber mode diameters (10.5, 8.5, and 6.5 μm) and four photodiode lengths. In this calculation only, we have taken the same mode diameter for 1.3- and 1.55-μm wavelength. The average quantum efficiency represents the photodiode performance and is defined as

$$\eta = \frac{1}{4}\left(\eta_{1.3}^{\mathrm{TE}} + \eta_{1.3}^{\mathrm{TM}} + \eta_{1.55}^{\mathrm{TE}} + \eta_{1.55}^{\mathrm{TM}}\right). \tag{5}$$

The results of Fig. 10, despite many optimizations, confirm that the photodiode length is a very important parameter for this structure. The fiber mode diameter has not, in comparison, a great influence. Precisely, for long photodiodes (150–200 μm), the performances obtained with a cleaved fiber are a little higher than those corresponding to smaller fiber modes, but it is the contrary for smaller photodiode lengths (50–100 μm). Moreover, the optimum fiber position depends on the photodiode length. Knowing that the waveguide surface position is located at $+5$ μm (shown in Fig. 10), the small photodiodes require the optical beam to be injected closer to the photodiode absorbing layer. These characteristics guided the choice of the second structure. The last aspect of the performances is that

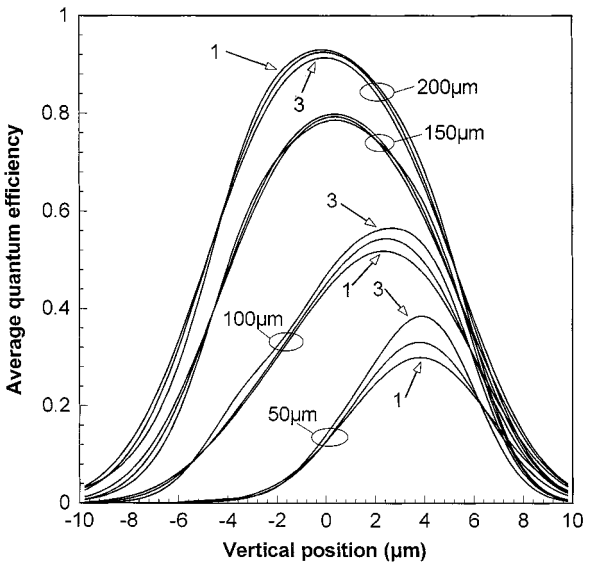

Fig. 10. Average quantum efficiency of the structure 1-50-0 for three different fiber mode widths (1:10.5 μm, 2:8.5 μm, 3:6.5 μm) and for four photodiode lengths: 50, 100, 150, and 200 μm. The position 0 μm is set 5 μm under the waveguide surface (vertical axis). When the position increases, the fiber moves toward the top of the device.

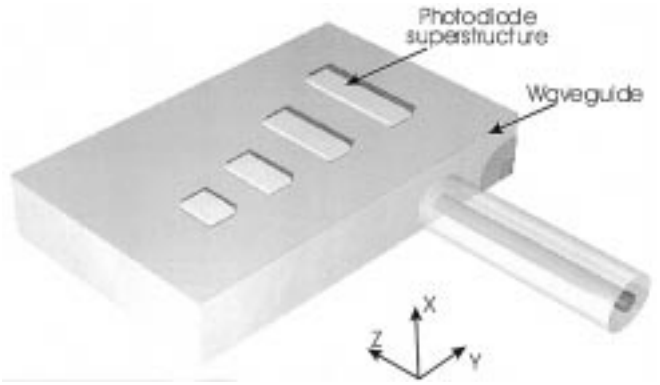

Fig. 11. Schematic of the fabricated device in front of the fiber with coordinates.

the alignment tolerance is quasi independent of the fiber mode width, but decreases with photodiode length.

Considering now the measurement procedure (see the schematic in Fig. 11), the optical fiber position was easy to find. The horizontal misalignment tolerance was not critical and the reproducibility of the measurements was very good, with a precision within 2%. Fig. 12 shows the device response efficiency versus fiber vertical position (axis X) with experiment–theory comparison at 1.30- and 1.55-μm wavelengths. In each case, experimental curves follow theoretical ones very well and there is a satisfactory experiment–theory agreement concerning sensibility and alignment tolerance. The difference can be due to small errors in the epitaxial structure, a wider fiber mode diameter at both wavelengths, the optical divergence of the optical beam issued from the fiber, or an error in the optical power calibration representing a few percent.

However, the measured performances are very good:

- responsivities of 1.03 and 0.86 A/W, respectively, at 1.55- and 1.3-μm wavelengths;

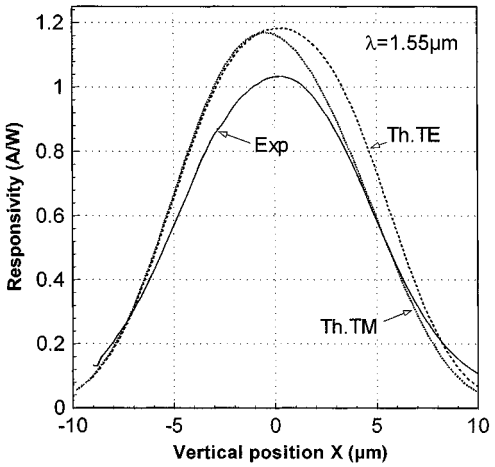

(a)

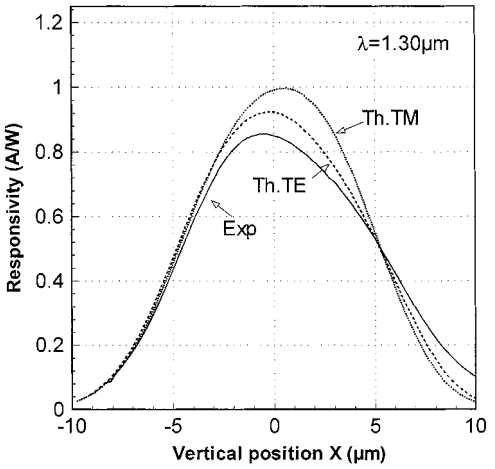

(b)

Fig. 12. Responsivity of the structure 1-50-0 in the vertical plane with experiment–theory comparison. The photodiode length is 200 μm. For each diagram, we plotted the experimental curve and the theoretical TE and TM curves.

- corresponding vertical alignment tolerances of 6.7 and 6.4 μm at -1 dB (11.0 and 10.7 μm at -3 dB);
- almost no polarization dependence (maximum 0.1 dB).

Despite the 2.5-Gb/s objective, we can have an insight in higher frequency potentialities. The active undoped layer of this structure is the GaInAs epilayer. The cutoff frequency is then related to the geometrical dimensions of this active region. With a photodiode width of 50 μm, the two last parameters to be considered are the thickness and the length. The calculated curves of Fig. 13 demonstrate the possibility of reducing the absorbing layer thickness without reducing the photodetector responsivity. This is a typical property of an evanescently coupled photodetector. However, in the case of the structure 1, the necessary photodiode length decrease will penalize the responsivity, as shown in Fig. 14. Several optimizations were made to define other structures with lower photodiode lengths. The solutions obtained have interesting performances (see Fig. 15) but the quantum efficiency falls below 0.9, and for lengths below 50 μm, there is a mismatch between the different requirements. The multiple optimizations we carried out did not allow to overcome this mismatch. Moreover, we also observe

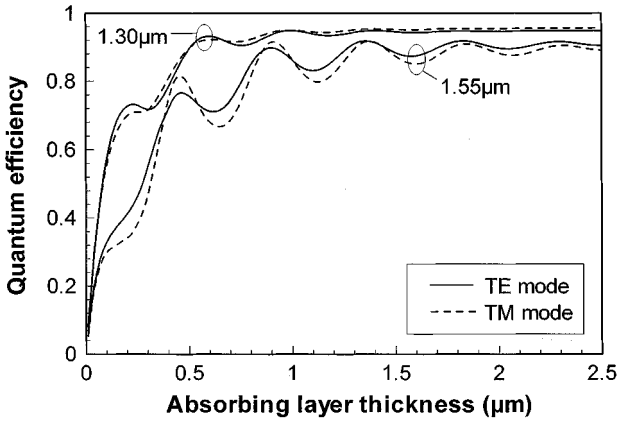

Fig. 13. Quantum efficiency of structure 1 versus absorbing-layer thickness for both wavelengths and optical polarizations.

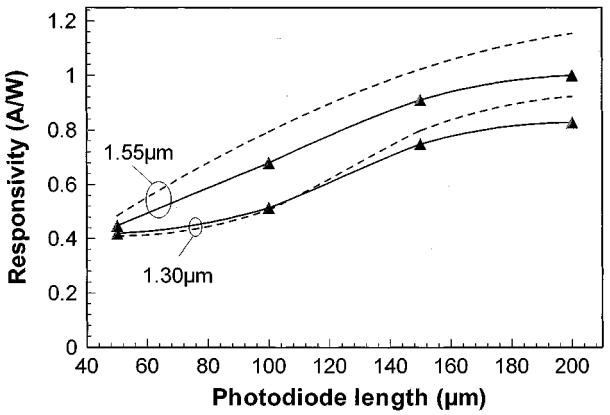

Fig. 14. Structure 1: responsivity versus photodiode length for both wavelengths and experiment–theory comparison (TE mode). Lines with symbols are experimental results and dashed lines theoretical results.

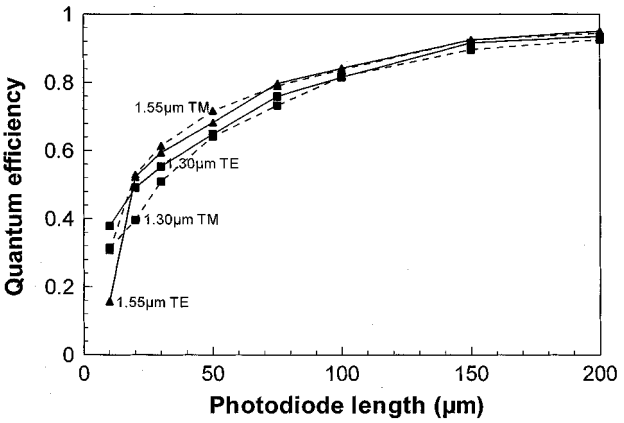

Fig. 15. Performances of the best optimized structures versus photodiode length. Each length corresponds to a photodetector structure, all structures are suitable for cleaved fiber.

a decrease of the alignment tolerance. All of these aspects, combined with the fact that a lensed fiber could be used in the fabrication of the optoelectronic modules, led us to consider a second structure with smaller optical beam injected closer to the waveguide surface. Overall, the modeling results we get demonstrate the possibility of obtaining quantum efficiency

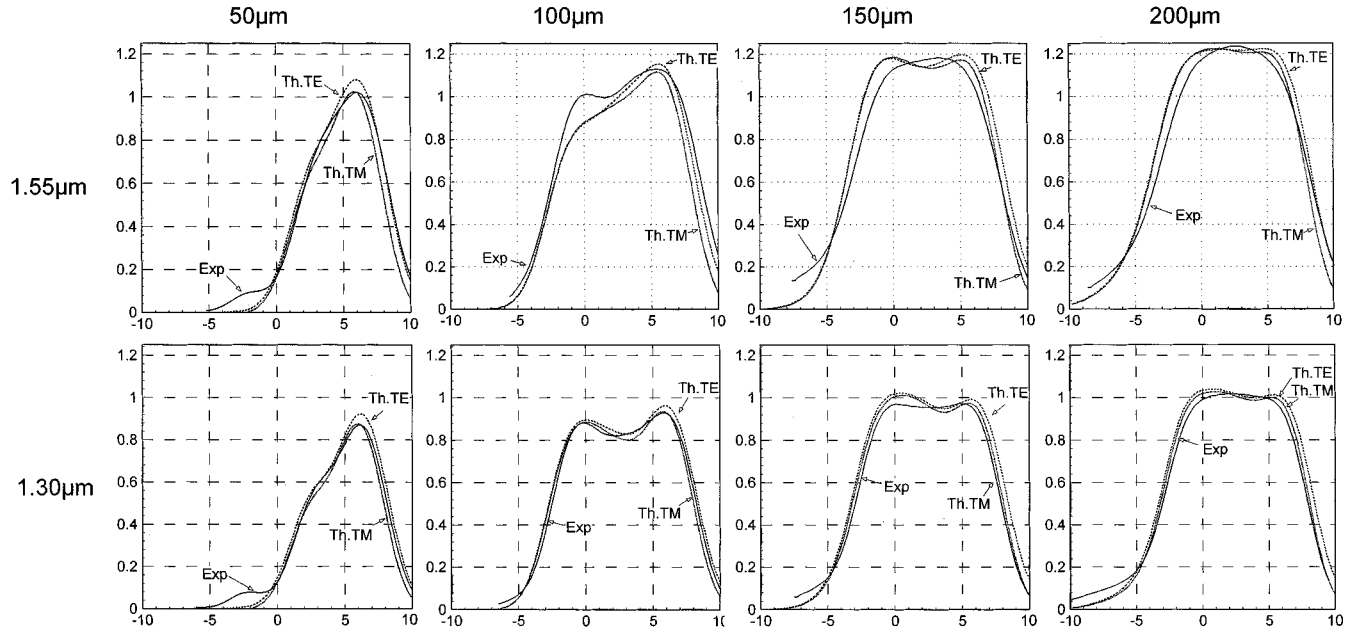

Fig. 16. Responsivity of the structure 2-0-0 in the vertical plane with experiment–theory comparison. Horizontal axis: vertical position in micrometers. Vertical axis: responsivity in amperes per watt. Above are the curves at 1.55 μm for the four photodiode lengths 50, 100, 150, 200 μm. Below are the same curves at 1.30 μm. For each graph, we plotted the experimental curve and the theoretical TE and TM curves.

greater than 80% at both wavelengths with a photodiode length of 75 μm. This is promising for devices that are side illuminated with a cleaved fiber.

C. Structure 2 for Lensed Fiber

Starting from this epitaxial structure, various photodetectors have been fabricated, with photodiode lengths of 50, 100, 150, and 200 μm and waveguide lengths of 0, 50, and 100 μm. The devices did not have antireflection coating. Because the photodiode is wide, the horizontal alignment tolerance is still high like for the previous structure. At first, in order to study the experiment–theory comparison, we tested photodetectors without input waveguide (the waveguide lengths L_1 and L_2 are equal to 0 μm). Fig. 16 presents the performances of this structure for both wavelengths and the four different photodiode lengths. Each graph presents the responsivity versus vertical position X with a comparison between experimental and theoretical (TE and TM modes) results. The experimental and theoretical results match very well. Moreover, as predicted by the model, the influence of optical polarization was negligible (lower than 0.1 dB). The position $+6$ μm corresponds to an illumination centerd on the GaInAs epilayer. For this reason, a maximum responsivity is obviously observed at this position. For a 50-μm photodiode length, the waveguide structure below the photodiode upper structure does not allow the light to be confined toward the absorbing epilayer because the photodiode is too short, but this problem is not encountered for longer photodiodes where a high responsivity is observed at the position $X = 0$ μm corresponding to the predicted waveguide center. Additionally, because of the possibility of directly illuminating the GaInAs layer through the cleaved facet, the vertical alignment tolerance measured for structures longer than 100 μm is higher than 8 μm (± 4 μm). However, this photodetector is not the most interesting, due to possible passivation problems. The second photodetector that we present has a 50-μm-long input waveguide and satisfies this last requirement. The same diagram as before is presented in Fig. 17 for this device. In this case, for 50-μm-long photodiode, the responsivity is acceptable when the fiber is centerd at $X = 0$ μm, and the performances are high for all lengths. As predicted by the model, the small photodetectors (50–100 μm) are more sensitive to optical polarization than are the longer ones (150–200 μm), but experimentally, this sensitivity does not exceed quantum efficiency for both wavelengths by more than a few percent. Moreover, for each graph, the measured responsivity at $+6$ μm is higher than the predicted one. This could be due to the light reinjected in the absorbing layer through the etched facet of the photodiode. We did not succeed in fitting this phenomenon systematically with our model. Obviously, the alignment tolerance is smaller than before, but it exceeds 5 μm (± 2.5 μm), which is more than convenient for the envisaged applications.

IV. Discussion and Conclusion

The design, optimization, and fabrication of evanescently coupled side-illuminated p-i-n photodetectors have been carried out in order to get highly reliable photodetectors suitable for hybrid surface integration. The aim of this work was, at the same time, to validate a design method adapted to complicated new guiding structures and to fabricate a new photodetector based on a multimode diluted waveguide. The theoretical properties of such waveguides, and particularly the possibility of obtaining large modes, make these structures promising in the field of integrated optics. However, they are complicated and cannot be designed using a separation-of-variables technique, especially in the case of a device that must satisfy numerous requirements, including wavelength and polarization. In this

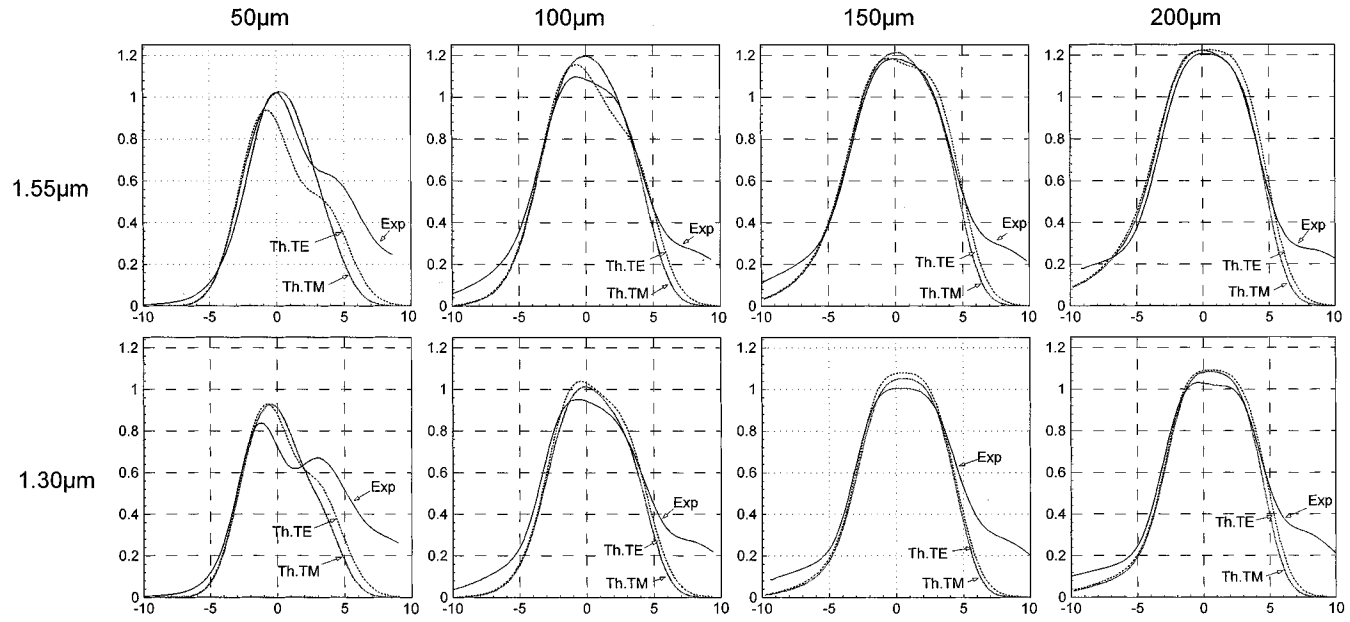

Fig. 17. Responsivity of the structure 2-50-0 in the vertical plane with experiment–theory comparison. Horizontal axis: vertical position in micrometers. Vertical axis: responsivity in amperes per watt. First row: curves at 1.55 μm for photodiode lengths 50, 100, 150, and 200 μm. Second row: same curves at 1.30 μm. For each graph, we plotted the experimental curve and the theoretical TE and TM curves.

TABLE IV
MAIN PERFORMANCES EXPERIMENTALLY OBSERVED IN THIS WORK

			λ = 1.55 µm		λ = 1.30 µm	
	Fibre	PD. length	R (A/W)	Δ (µm)	R (A/W)	Δ (µm)
Struct. 1-50-0	cleaved	200 µm	1.03	6.5	0.86	6.5
Struct. 2-0-0	lensed	200 µm	1.22	8.6	1.02	8.6
Struct. 2-50-0	lensed	200 µm	1.21	5.9	1.05	5.4
Struct. 2-50-0	lensed	100 µm	1.10	5.7	0.93	6.0

context, the genetic algorithm becomes an important tool allowing us to overcome the problem. As is well known, the calculated solutions are not the best possible ones, and only provide a certain fit to programmed requirements. The final solutions and performances depend on the fitness formulation and on the preliminary definition of the search space. Our objective was to design a photodetector for 2.5-Gb/s applications. In our case, because the active area is 50×200 μm^2, and the absorbing layer thickness is 2 μm, the cutoff frequency related to capacitance effect is 5.5 GHz whereas that related to transit time limitation is 14.8 GHz [1]. Consequently, the resulting device cutoff frequency is close to 5 GHz [43], dominated by capacitance effect. The performances obtained are of high level as summarized in Table IV; R is the responsibility and Δ is the vertical alignment tolerance. For the first structure, the experimental quantum efficiency is close to 0.83 for both wavelengths. The experiment–theory comparison is good for all requirements. For the second structure, the excellent experimental results agree even better with predictions. We think that the performances obtained for cleaved fiber can be improved. All of the results confirm the accuracy of the BPM and demonstrate the capability of the photodetector structure.

In order to improve the dynamic behavior, the main objective must be the photodiode length and width reduction in order to reduce the capacitance. Structure 2 keeps a quantum efficiency higher than 0.9 until it reaches a photodiode length of 75 μm, and our optimization results give a possible structure for cleaved fiber with 100-μm-long photodiode. Moreover, a taper can be designed to laterally confine the light and decrease the photodiode width. Concerning the transit time limitation, the active region thickness can be reduced if the matching epilayer materials and thicknesses are optimized. All of these aspects allow to predict a possible cutoff frequency higher than 30 GHz while keeping a very high responsivity and alignment tolerance for both wavelengths. Obviously, however, when the photodiode length decreases, better performances can be expected from structures designed for only one wavelength.

ACKNOWLEDGMENT

The authors would like to thank S. Mc Murtry for interesting discussions and helpful participation in the fabrication of the manuscript.

REFERENCES

[1] K. Kato, "Ultrawide-band/high-frequency photodetectors," *IEEE Trans. Microwave Theory Tech.*, vol. 47, pp. 1265–1281, July 1999.
[2] H. Mawatari, M. Fukuda, K. Kato, T. Takeshita, M. Yuda, A. Kozen, and H. Toba, "Reliability of planar waveguide photodiodes for optical subscriber systems," *J. Lightwave Technol.*, vol. 16, pp. 2428–2434, Dec. 1998.
[3] K. Kato, S. Hata, A. Kozen, J. Yoshida, and K. Kawano, "Highly efficient 40 GHz waveguide InGaAs PIN photodiode employing multimode waveguide structure," *IEEE Photon. Technol. Lett.*, vol. 3, pp. 820–822, Sept. 1991.
[4] D. Wake, T. P. Spooner, D. D. Perrin, and I. D. Henning, "50 GHz InGaAs edge-coupled PIN photodetector," *Electron. Lett.*, vol. 27, pp. 1073–1075, June 1991.

[5] K. Kato, A. Kozen, Y. Muramoto, Y. Itaya, T. Nagatsuma, and M. Yaita, "110 GHz 50% efficiency mushroom mesa waveguide PIN photodiode for 1.55 μm wavelength," *IEEE Photon. Technol. Lett.*, vol. 6, pp. 719–720, June 1994.
[6] Y. Wey, K. Giboney, J. Bowers, M. Rodwell, P. Silvestre, P. Thiagarajan, and G. Robinson, "108 GHz GaInAs/InP PIN photodiodes with integrated bias tees and matched resistors," *IEEE Photon. Technol. Lett.*, vol. 5, pp. 1310–1312, Nov. 1993.
[7] I. Tan, C. Sun, K. Giboney, J. Bowers, E. L. Hu, B. Miller, and R. Capik, "120 GHz long wavelength low capacitance photodetector with an air-bridged coplanar metal waveguide," *IEEE Photon. Technol. Lett.*, vol. 7, pp. 1477–1479, Dec. 1995.
[8] J. Harari, F. Journet, O. Rabii, G. H. Jin, J. P. Vilcot, and D. Decoster, "Modeling of waveguide PIN photodetectors under very high optical power," *IEEE Trans. Microwave Theory Tech.*, vol. 43, pp. 2304–2310, Sept. 1995.
[9] D. J. Vezzetti and M. Munowitz, "Design of strip-loaded optical waveguides for low-loss coupling to optical fibers," *J. Lightwave Technol.*, vol. 10, pp. 581–586, 1992.
[10] K. Kasaya, O. Mitomi, M. Naganuma, Y. Kondo, and Y. Noguchi, "A simple laterally tapered waveguide for low loss coupling to single mode fibers," *IEEE Photon. Technol. Lett.*, vol. 5, pp. 345–347, Mar. 1993.
[11] B. Mersali, F. Ghirardi, J. Brandon, G. H. Gruyer, and A. Carenco, "Low-loss fiber-matched diluted multiple quantum well waveguides," *IEE Proc. Optoelectron. J*, vol. 141, pp. 296–302, Oct. 1994.
[12] J. F. Vinchant, P. Pagnod-Rossiaux, J. Le Bris, A. Goutelle, H. Bissessur, and M. Renaud, "Low-loss fiber-chip coupling by InGaAsP/InP thick waveguides for guided-wave photonic integrated circuits," *IEEE Photon. Technol. Lett.*, vol. 6, pp. 1347–1349, Nov. 1994.
[13] T. Brenner, M. Bachmann, and H. Melchior, "Vertically tapered InGaAsP/InP waveguides for highly efficient coupling to flat end single-mode fibers," *Appl. Phys. Lett.*, vol. 65, pp. 798–800, Aug. 1994.
[14] O. Mitomi, K. Kasaya, Y. Tohmori, Y. Suzaki, H. Fukano, Y. Sakai, M. Okamoto, and S. Matsumoto, "Optical spot-size converters for low-loss coupling between fibers and optoelectronic semiconductor devices," *J. Lightwave Technol.*, vol. 14, pp. 1714–1719, July 1996.
[15] O. Mitomi, N. Yoshimoto, K. Magari, T. Ito, Y. Kawaguchi, Y. Suzaki, Y. Tohmori, and K. Kasaya, "Analysing the polarization dependance in optical spot-size converter by using a semivectorial finite element beam propagation method," *J. Lightwave Technol.*, vol. 17, pp. 1255–1261, July 1999.
[16] H. Kaufmann, P. Buchmann, R. Hirter, H. Melchior, and G. Guekos, "Self-adjusted permanent attachment of fibers to GaAs waveguide components," *Electron. Lett.*, vol. 22, pp. 712–714, June 1986.
[17] D. Leclerc, P. Brosson, F. Pommereau, R. Ngo, P. Doussière, F. Mallécot, P. Gavignet, I. Wamsler, G. Laube, W. Hunziker, W. Vogt, and H. Melchior, "High performance semiconductor optical amplifier array for self aligned packaging using Si V-groove flip-chip technique," *IEEE Photon. Technol. Lett.*, vol. 7, pp. 476–478, May 1995.
[18] J. Stulemeijer, A. F. Bakker, I. Moerman, F. H. Groen, and M. K. Smit, "InP-based spotsize converter for integration with switching devices," *IEEE Photon. Technol. Lett.*, vol. 11, pp. 81–83, Jan. 1999.
[19] H. Nakamura, M. Shishikura, S. Tanaka, Y. Matsuoda, T. Ono, T. Miyazaki, and S. Tsuji, "High responsivity, low dark current, and highly reliable operation og InGaAlAs waveguide photodiodes for optical hybrid integration," *IEICE Trans. Electron.*, vol. E80-C, pp. 41–46, Jan. 1997.
[20] K. Kato, M. Yuda, A. Kozen, Y. Muramoto, K. Noguchi, and O. Nakajima, "Selective area impurity doped planar edge coupled waveguide photodiode (simple WGPD) for low cost, low power consumption optical hybrid modules," *Electron. Lett.*, vol. 32, pp. 2078–2079, Oct. 1996.
[21] T. Takeuchi, T. Nakata, M. Tachigori, K. Makita, and K. Taguchi, "Design and fabrication of a waveguide photodiode for 1.55 μm band access receivers," in *Proc. 10th Int.. Conf. Indium Phosphide Related Materials*, May 1998, pp. 262–263.
[22] K. Kato, R. Furukawa, T. Terashima, and H. Takano, "Large coupling tolerance side-illuminated mirror photodiode for low-cost surface hybrid integration," *IEEE Photon. Technol. Lett.*, vol. 11, pp. 709–711, June 1999.
[23] H. Fukano, Y. Muramoto, and Y. Matsuoda, "High speed and high output voltage edge illuminated refracting facet photodiode," *Electron. Lett.*, vol. 35, pp. 1581–1582, Sept. 1999.
[24] A. Umbach, D. Trommer, G. G. Mekonnen, W. Ebert, and G. Unterbörsch, "Waveguide integrated 1.55 μm photodetector with 45 GHz bandwidth," *Electron. Lett.*, vol. 32, pp. 2143–2145, Nov. 1996.
[25] G. Unterbörsch, A. Umbach, D. Trommer, and G. G. Mekonnen, "70 GHz long-wavelength photodetector," in *Proc. 23rd Eur. Conf. Optical Communications (ECOC'97)*, 1997, pp. 25–28.
[26] G. Wanlin, L. Giraudet, J. P. Praseuth, A. Miras, and E. Legros, "High responsivity side illuminated AlGaInAs PIN photodiode for 40 Gbit/s-40 GHz applications," in *Proc. 23rd Eur. Conf. Optical Communications (ECOC'97)*, vol. 2, 1997, pp. 163–166.
[27] L. Giraudet, F. Banfi, S. Demiguel, and G. H. Gruyer, "Optical design of evanescently coupled, waveguide-fed photodiodes for ultrawide-band applications," *IEEE Photon. Technol. Lett.*, vol. 11, pp. 111–113, Jan. 1999.
[28] J. Harari and V. Magnin, "Modeling and optimization of optoelectronic devices," in *Proc. ESSDERC'99*, 1999, pp. 103–110.
[29] J. H. Holland, *Adaptation in Natural and Artificial Systems*. Cambridge, MA: M.I.T. Press, 1975.
[30] T. Bäck, U. Hammel, and H. P. Schwefel, "Evolutionary computation: Comments on the history and current state," *IEEE Trans. Evolutionary Comput.*, vol. 1, pp. 3–17, Apr. 1997.
[31] D. E. Goldberg, *Genetic Algorithms in Search, Optimization and Machine Learning*. Reading, MA: Addison-Wesley, 1989.
[32] D. B. Fogel, "Evolutionary computation: A new transactions," *IEEE Trans. Evolutionary Comput.*, vol. 1, p. 1, Apr. 1997.
[33] Y. Chung and N. Dagli, "An assessment of finite difference beam propagation method," *IEEE J. Quantum. Electron.*, vol. 26, pp. 1335–1339, Aug. 1990.
[34] W. P. Huang, C. L. Xu, S. T. Chu, and S. K. Chaudhuri, "The finite-difference beam propagation method: Analysis and assessment," *J. Lightwave Technol.*, vol. 10, pp. 295–305, 1992.
[35] C. M. Fonseca and P. J. Fleming, "An overview of evolutionary algorithms in multiobjective optimization," *Evolutionary Comput.*, vol. 3, pp. 1–16, 1995.
[36] D. Beasley, D. R. Bull, and R. R. Martin, "An overview of genetic algorithms: Part 2, research topics," *Univ. Comput.*, vol. 15, no. 4, pp. 170–181, 1993.
[37] T. Bäck, "Self-adaptation in genetic algorithms," in *Proc. 1st Eur. Conf. Artificial Life*, 1992, pp. 263–271.
[38] B. Broberg and S. Lindgren, "Refractive index of $In_{1-x}Ga_xAs_yP_{1-y}$ layers and InP in the transparent wavelength region," *J. Appl.Phys.*, vol. 55, pp. 3376–3381, May 1984.
[39] E. Gini and H. Melchior, "The refractive index of InP and its temperature dependence in the wavelength range from 1.2 μm to 1.6 μm," in *Proc. IPRM'96*, pp. 594–597.
[40] D. Hahn, O. Jaschinski, H.-H. Wehmann, A. Schlachetzki, and M. Von Ortenberg, "Electron-concentration dependence of absorption and refraction in n-$In_{0.53}Ga_{0.47}As$ near the band-edge," *J. Electron. Mater.*, vol. 24, no. 10, pp. 1357–1361, 1995.
[41] L. Chusseau, P. Martin, C. Brasseur, C. Alibert, P. Hervé, P. Arguel, F. Lozes-Dupuy, and E. V. K. Rao, "Carrier-induced change due to doping in refractive index of InP: Measurements at 1.3 and 1.5 μm," *Appl. Physics Lett.*, vol. 69, no. 20, pp. 3054–3056, Nov. 1996.
[42] B. Reid, R. Maciejko, and A. Champagne, "Absorption and index of refraction for the modeling of InGaAsP/InP photonic devices," *Can. J. Phys.*, vol. 71, pp. 410–416, 1993.
[43] L. Giraudet, J. Harari, V. Magnin, P. Pagnod, E. Boucherez, J. Decobert, J. Bonnet-Gamard, D. Carpentier, C. Jany, S. Blache, and D. Decoster, "High speed evanescently coupled PIN photodiodes for hybridization on silicon platform optimized with genetic algorithm," *Electron. Lett.*, vol. 37, pp. 973–975, July 2001.

Vincent Magnin was born in Lille, France, in 1971. He received the engineer degree from the Lille University Engineering School, Lille, in 1994 and the Ph.D. degree from Lille University, Lille, in 1998.

In 1998, he joined the Institut d'Electronique et de Microélectronique du Nord (IEMN), Département Hyperfréquences et Semiconducteurs (DHS), Villeneuve d'Ascq, France. He is currently Assistant Professor in the Materials Science Department at the Lille University Engineering School. His current research activities focus on modeling and optimization of photodetectors and optical switches, particularly the problem of the optimization methods used in the optoelectronic field.

Louis Giraudet was born in Paris, France, in 1962. He received the Ph.D. degree from the University of Paris at Orsay, Paris, in 1988. His Ph.D. dissertation was on InP-based heterojunction field-effect transistors.

In 1990, he joined France Télécom-CNET, where he was involved in research on InP-based optoelectronics for optical fiber telecom applications. In particular, his work focused on integrated photoreceivers and optoelectronic integrated circuits. In 1995, he was in charge of a research group working on high-speed avalanche photodiodes and p-i-n photodiodes. In 1998, he joined Opto+, Marcoussis, France, where he was in charge of research in waveguided photodetectors, and now is involved in high-speed optoelectronic device characterization.

Joseph Harari was born in Enghien, France, in 1961. He received the engineer degree from the Polytechnic institute of Grenoble, Grenoble, France, and the Ph.D. degree from Lille University, Lille, France, in 1985 and 1991, respectively.

In 1992, he joined the Optoelectronic group of the Institut d'Electronique et de Microélectronique du Nord (IEMN). He is currently Assistant Professor at the Lille University Engineering School, Lille. His current activities focus on the simulation, design, and optimization of optoelectronic devices for millimeter-wave applications, integrated optics, and optical interconnections.

J. Decobert, photograph and biography not available at the time of publication.

P. Pagnot, photograph and biography not available at the time of publication.

E. Boucherez, photograph and biography not available at the time of publication.

Didier Decoster was born in Lille, France, in 1948. He received the Ph.D. degree in electronics and physical science from the University of Lille, Lille.

He is currently a professor at the Engineering School of the University of Lille in the Material Science Department. His research activities are with the Institut d'Electronique et de Microélectronique du Nord (IEMN), Marcoussis, France, where he is the leader for the electromagnetism, optoelectronics, and optoacoustics group. His research activities include optoelectronic and photonic components and integrated circuits on III–V materials, microwave applications of optics, and optical interconnections.